frontiers in Materials

ORIGINAL RESEARCH
published: 13 January 2022
doi: 10.3389/fmats.2021.819961

Compressive Behavior and Analytical Model of Ultra-Early Strength Concrete-Filled FRP Tube With Zero Curing Time

Yue Liu, Jia-Zhan Xie and Jing-Liang Yan*

The Key Laboratory of Urban Security and Disaster Engineering of Ministry of Education, Beijing University of Technology, Beijing, China

OPEN ACCESS

Edited by:
Lik-ho Tam,
Beihang University, China

Reviewed by:
Huawen Ye,
Southwest Jiaotong University, China
Tao Wu,
Technical University Dresden, Germany

****Correspondence:***
Yue Liu
yliu@bjut.edu.cn

Specialty section:
This article was submitted to Structural Materials, a section of the journal Frontiers in Materials

Received: *22 November 2021*
Accepted: *06 December 2021*
Published: *13 January 2022*

Citation:
Liu Y, Xie J-Z and Yan J-L (2022) Compressive Behavior and Analytical Model of Ultra-Early Strength Concrete-Filled FRP Tube With Zero Curing Time. Front. Mater. 8:819961. doi: 10.3389/fmats.2021.819961

Fiber-reinforced polymer (FRP) has been widely used in civil engineering due to its light weight, high strength, convenient construction, and strong corrosion resistance. One of the important applications of FRP composites is the concrete-filled FRP tube (CFFT), which can greatly improve the compressive strength and ductility of concrete as well as facilitate construction. In this article, the compressive performances of a normal concrete-filled FRP tube (N-CFFT) column with 5-hour curing time and an ultra-early strength concrete-filled FRP tube (UES–CFFT) column with zero curing time were studied by considering the characteristics of rapid early strength improvement of ultra-early strength concrete and the confinement effect of the FRP tube. Monotonic axial compression tests were carried out on 3 empty FRP tubes (FTs) without an internal filler and 6 CFFT (3 N-CFFTs and 3 UES-CFFTs) specimens. All specimens were cylinders of 200 mm in diameter and 600 mm in height, confined by glass fiber–reinforced polymer (GFRP). Test results indicated that the compressive bearing capacity of the specimens increased significantly by adopting the ultra-early strength concrete as the core concrete of the CFFT, although the curing time was zero. It was also shown that the compressive behavior of the UES–CFFT specimens with zero curing time increased significantly than that of the N-CFFT specimens with 5-hour curing time because the former was able to achieve rapid strength enhancement in a very short time than the latter. The ultimate compressive strength of UES–CFFT specimens with zero curing time reached 78.3 MPa, which was 66.2 and 97.2% higher than that of N-CFFT with 5-hour curing time and FT specimens, respectively. In addition, a simple confinement model to predict the strength of UES–CFFT with zero curing time in ultimate condition was introduced. Compared with the existing models, the proposed model could predict the ultimate strength of UES–CFFT specimens with zero curing time with better accuracy.

Keywords: ultra-early strength concrete (UESC), FRP, concrete-filled FRP tube, mechanical test, strength model

1 INTRODUCTION

The application of fiber-reinforced polymer (FRP) composites for strengthening and rehabilitation of concrete structures is gaining increasing popularity in the civil engineering community. FRP tubes, made of the long fiber filaments infiltrated with resin and winding on the core mold with a certain angle, are widely used in practical projects. The concrete-filled FRP tubes (CFFTs) can be used as compression members such as piers, piles, and towers of bridges. Among them, the FRP tube provides longitudinal and transverse constraints to the core concrete, which makes the core concrete in a three-way stress state and hence greatly improving the compressive strength and ductility. Furthermore, the existence of core concrete can delay and avoid the local buckling of the FRP tube, which is a thin-walled member, and guarantee the full play of FRP performance (Xie et al., 2012). The CFFT has many advantages compared with normal reinforced concrete column or concrete-filled steel tube column, including 1) the FRP tube is more efficient than normal steel stirrups to confine the core concrete, hence increasing the bearing capacity and ductility of the column; 2) the FRP tube can be used as a non-dismantling template during construction, which saves the template cost and accelerates the construction speed; and 3) the FRP tube has excellent corrosion resistance and can provide a protective shell for the core concrete, especially suitable for corrosive environments such as oceans (Wu, 2007). The CFFT was first proposed by Mirmiran and Shahawy (Mirmiran and Shahawy, 1995) in 1995. Mirmiran et al. (Mirmiran and Shahawy, 1997; 1998; Mirmiran et al., 2001) conducted experimental studies on the axial compression performance of the CFFT specimens and discussed the influence of significant factors (e.g., column section shape, FRP tube thickness, concrete strength, slenderness ratio, and other parameters) on the axial compression performance. Li and Xue (Li and Xue, 2004) obtained the stress–strain relationship and bending moment–curvature curve of the CFFT under different stress conditions by carrying out bending, axial compression, and eccentric compression tests on 14 specimens. The curve was a two-fold line, in which the first stiffness was controlled by the concrete section and the second stiffness was controlled by the FRP tube. Saafi et al. (Saafi et al., 1999) proposed a CFFT model based on the FRP cloth restraint concrete column model. Fam and Rizkalla (Fam et al., 2001) utilized the relationship between the axial strain and lateral strain of concrete under hydrostatic pressure to calculate the lateral deformation of the CFFT and established the mechanical model of the CFFT by using the progressive increment method. Wu et al. (Wu and Lv, 2003; Wu G. et al., 2006) studied the stress–strain relationship and established the calculation model of the CFFT with or without softening section, respectively. Teng et al. (Teng et al., 2006) proposed the FRP tube–concrete–steel tube composite column (DSTC), which was composed of the FRP outer tube and steel inner tube and concrete filled between them. The three materials worked together, maximizing the strengths, and avoiding the weaknesses, so that the FRP tube composite column generated many excellent mechanical properties. Zhuo and Fan (Zhuo and Fan, 2005) studied the seismic performance of FRP tube concrete bridge piers through pseudo-static and shaking table tests. The results showed that FRP tube concrete bridge piers had good seismic performance and could overcome the seismic vulnerability defects of normal reinforced concrete bridge piers.

In summary, most existing studies are on the normal concrete-filled FRP tube (N-CFFT). As far as the authors know, no scholar has studied the compressive performance of the ultra-early strength concrete-filled FRP tube (UES-CFFT) with zero curing time so far. In view of this, the uniaxial compression tests on three types of specimens (FT, N-CFFT specimens with 5-hour curing time, and UES–CFFT specimens with zero curing time) were conducted, and the experimental results were analyzed in detail in this article. Furthermore, a modified simple model to predict the strength response of UES–CFFT with zero curing time in ultimate condition was proposed based on an existing FRP confined concrete model.

2 MATERIALS

2.1 Core Concrete

Two types of core concrete were manufactured for the present experimental program, namely, NC (normal concrete) and UESC (ultra-early strength concrete), which would be applied to the N-CFFT and UES–CFFT specimens, respectively. The NC used in the test was provided by local concrete suppliers with the mix ratio of water:cement:sand: gravel = 0.38:1:1.11:2.72. The selective cement of NC was normal portland cement (NPC), the grade of sands was medium sand, and the grain diameters of gravels were in the range of 5–25 mm. The UESC was prepared in the laboratory with the same mix ratio as NC. Both the grade of sands and the grain diameters of gravels were exactly identical. The difference between them was that the selective cement of UESC was fast-hardening sulfoaluminate cement (FHSC), which could quickly promote the early strength of concrete. The images of NPC and FHSC on site are shown in **Figure 1**. Besides, in order to greatly improve the fluidity of concrete and make the entire structure more stable, an appropriate amount of water reducer and retarder was added. To remove undesired air voids from concrete to achieve high strength, a moderate defoamer was also added to concrete. The mix designs of the NC and UESC adopted are listed in **Table 1**.

Furthermore, six control cylinders with 100 by 200 mm dimensions were cast from the NC and UESC mixes and tested in parallel to the CFFT specimens (including N-CFFT and UES–CFFT) to determine the compressive strength. Three NC control cylinder specimens with 5-hour curing time and three UESC control cylinder specimens with zero curing time were prepared and tested. The in-place strength of unconfined concrete (f'_{co}) in each type of specimens and the corresponding axial strain (ε_{co}) are given in **Table 2**. The (ε_{co}) values of all control cylinders were not measured directly but calculated using the expression given by Tasdemir et al. (Tasdemir et al., 1998).

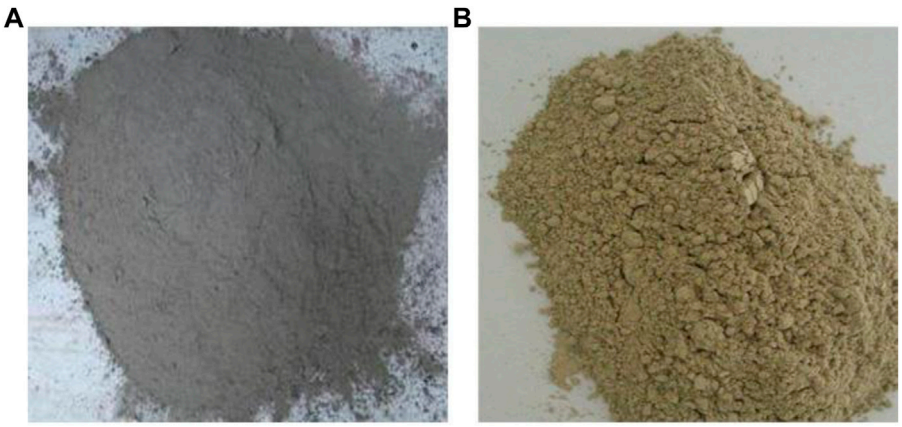

FIGURE 1 | Images of NPC and FHSC on site, **(A)** Normal portland cement (NPC), **(B)** fast-hardening sulfoaluminate cement (FHSC).

TABLE 1 | Mix designs of NC and UESC.

	NC		UESC	
	Type	**Value (kg/m^3)**	**Type**	**Value (kg/m^3)**
Cement	NPC	461	FHSC	461
Sand	Medium sand	512	Medium sand	512
Gravel	5–25 mm (D_g)	1,252	5–25 mm (D_g)	1,252
Water	—	175	—	175
Admixture	—	—	Water reducer	1.2
	—	—	Defoamer	0.1
	—	—	Retarder	1.0
Sum	—	2,400	—	2,402.3

D_g *represents the grain diameter of gravel.*

TABLE 2 | Test results of the control concrete cylinders.

Concrete cylinder	$f_{,co}$ **(MPa)**	ε_{co}
NC-1	1.8	0.10
NC-2	1.9	0.09
NC-3	1.8	0.11
UESC-1	8.1	0.11
UESC-2	7.8	0.10
UESC-3	8.3	0.12

2.2 FRP Tubes

FRP tubes used in this study were produced by means of the filament winding process where the necessary raw materials mainly included reinforcing fibers (60%) and resin (40%). The thickness of all FRP tubes tested was 6 mm. **Figure 2** shows a typical winding process, which adopts wet winding and a typical rotating mandrel as the mold for winding fibers. First, the fibers extracting from the creel, after passing through the guiding tension roller, were given a wet-out bath where they were impregnated with resin. Then the fibers after the wet bath were assembled into a bundle through the directional slot. Finally, under certain tension control, a rotating device was used to wind the bundled fibers on the mold at a preset angle (60°). In the process of winding, the fiber position should be stable and skid-proof; and the surface of the mold should be evenly and continuously covered, so that the adjacent fibers were neither overlapped nor separated to the required thickness. The product was demolded after curing.

The mechanical properties of the FRP tubes provided by the manufacturer are given in **Table 3**, which were obtained from the test according to ASTM D3171-15 "Standard Test Methods for Constituent Content of Composite Material" (ASTM, 2015). In order to keep the consistency of the experimental specimens, all composites were from the same source and the same batch.

3 EXPERIMENTAL PROGRAM

3.1 Specimen Preparation

In order to investigate the compressive performances of the N-CFFT with 5-hour curing time and UES–CFFT with zero curing time, nine cylinder specimens (3 FT specimens, 3 N-CFFT specimens with 5-hour curing time, and 3 UES–CFFT specimens with zero curing time) were subjected to uniaxial compression tests. Since the early strength of NC had not yet generated just after pouring, N-CFFT could not be placed on the loading device at this time. Therefore, through simple tests and observation on the N-CFFT with the different curing time (1, 2, 3, 4, 5h, respectively), it was found that the specimens cured for 5 h could satisfy the strength and plasticity required by the test, so it was finally decided to cure the N-CFFT for 5 hours. All specimens were short columns with a length-to-diameter ratio of 3. The diameter of each specimen was 200 mm, and the height was 600 mm. The details of all the test specimens are given in **Table 4**.

3.2 Test Procedure

As shown in **Figure 3A**, all specimens were tested on a compression test machine with a maximum carrying capacity of 3,000 kN. The equipment had sufficient capacity and stiffness for such tests, and it was also equipped with computer control and a data acquisition system. The load was exerted on the cylinder

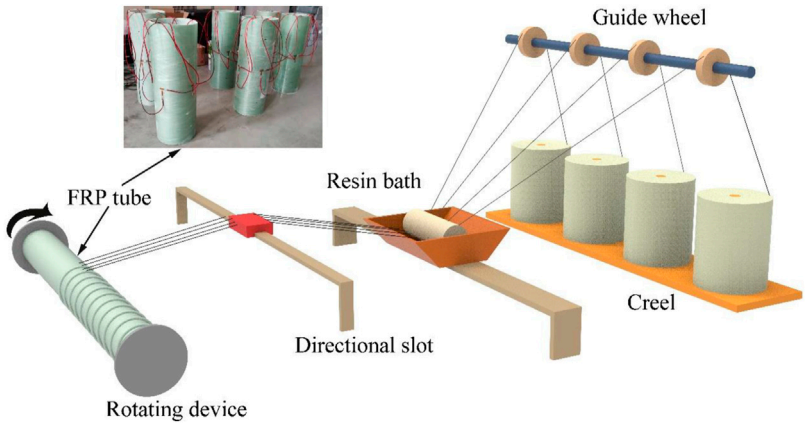

FIGURE 2 | Manufacturing process of FRP tubes.

TABLE 3 | Material properties of FRP tubes.

Fiber parameter	Properties provided by the manufacturer
Density, (g/cm^3)	2.51
Poisson ratio	0.30
Circumferential tensile strength, f_{ct} (MPa)	210
Axial tensile strength, f_{at} (MPa)	130
Circumferential elastic modulus, E_c (GPa)	17
Axial elastic modulus, E_a (GPa)	10

specimens through a square pad slightly larger than the cross section of the specimens. Three linear variable differential transformers (LVDTs) were connected to the steel block to record the axial deformations of each specimen, which were distributed at equal intervals along the circumference of the specimen. Four axial strain gauges and four lateral strain gauges were arranged equidistantly along the circumferential direction at the middle height of the outer surface of FRP tube, so as to measure the axial and lateral strains during loading. The details of arrangement of the three LVDTs and eight strain gauges are shown in **Figure 3B**. Uniaxial compression was adopted in the test, and the axial displacement rate was set to 4 mm/min. The results to be measured included axial load, compression displacement of each specimen, and axial and lateral strains at four measuring points on the outer surface of the FRP tube. Besides, the upper and lower ends of all tested specimens were wrapped with a CFRP cloth to prevent damage due to stress concentration at the end.

3.3 Test Results and Discussion

3.3.1 Failure Modes

Figure 4 shows the typical failure modes of the three types of specimens (A, B, and C represent FT, N-CFFT, and UES–CFFT specimens, respectively). When the FT specimen was loaded (**Figure 4A**), as the load increased, the transverse tensile stress of the FRP tube increased and cracks began to appear in the middle upper part of the FRP tube. The development trend of the cracks was not the overall cracking around the FRP tube, but the slight cracks appeared at some positions and gradually extended along the circumferential direction to both sides. With the continuous increase in load, the loading end of the specimen gradually showed obvious eccentricity, resulting in the steel plate which was above the specimen to tilt. Finally, the cracks gradually developed seriously, and the whole specimen was damaged, white fibers leaking out were clearly visible in the cracks. When the N-CFFT specimen was loaded (**Figure 4B**), since the core concrete had not yet completed solidification and formed sufficient strength, the FRP tube was loaded first and the core concrete was compacted with the increase in load. Moreover, there was a small amount of water flowed out of the bottom of the specimen. Then both the FRP tube and core concrete had compression together, and the core concrete begun to deform slightly. The FRP tubes laterally restrained the core concrete and then the tube cracked, causing damage to the specimen. The

TABLE 4 | Details of test specimens.

Specimen type	Core concrete	D (mm)	H (mm)	Thickness of FRP tube (mm)	Curing time (h)	Number of specimens
FT	—	200	600	6	—	3
N-CFFT	NC	200	600	6	5	3
UES-CFFT	UESC	200	600	6	0	3

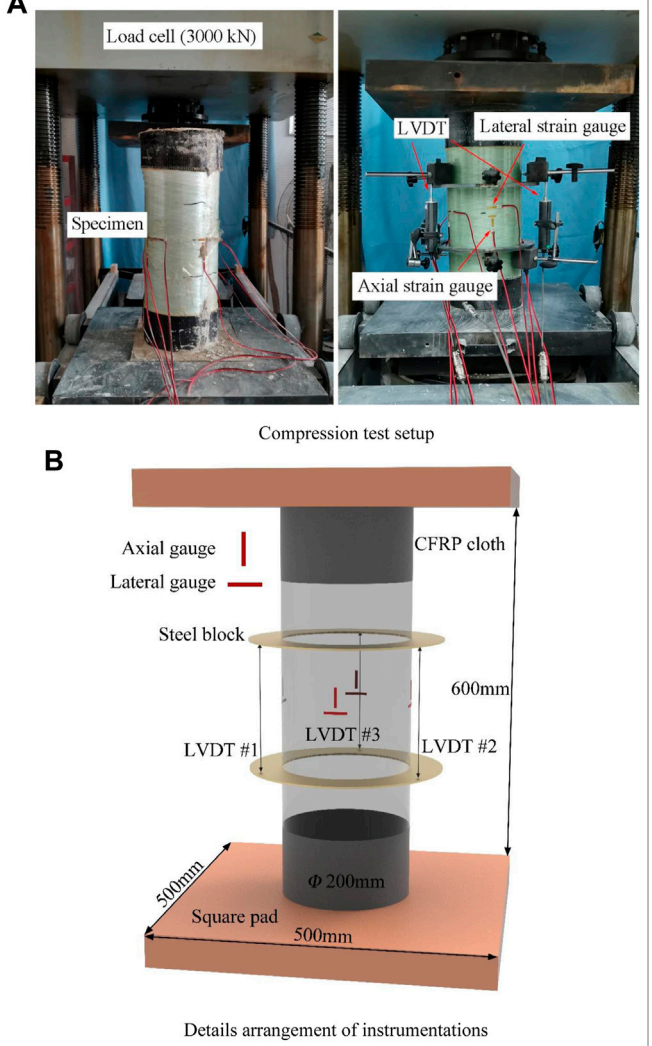

FIGURE 3 | (A) Compression test setup and **(B)** detailed arrangement of instrumentations.

eccentricity also occurred after the cracks appeared in the later stage of the loading. One was due to the unevenness of the concrete mortar, and the other was due to the formation of a weak surface after the cracking of the FRP tube. However, because the core concrete was compressed into a solid, the eccentricity of the N-CFFT specimen was not serious than that of the FT specimen. When the UES–CFFT specimen was loaded (**Figure 4C**), since the strength of the UESC could quickly increase in a short time, both the FRP tube and core concrete were under compression from the beginning of loading, and eventually the specimen was also damaged due to the cracking of the FRP tube. Similar to the destruction of N-CFFT specimen above, the eccentricity of the UES–CFFT specimen was a little smaller than that of the N-CFFT specimen. It should be noted that from the FT, N-CFFT, to the UES–CFFT specimens, the crack height of the FRP tubes was continuously increasing, and the length of the cracks ranged from the FT specimen (close to the entire circumference of the specimen) to the N-CFFT specimen (approximately 1/3 of the entire circumference of the specimen), and finally to the UES–CFFT specimen (approximately 1/5 of the entire circumference of the specimen). Besides, from the white area of the cracks, the width of the cracks was constantly getting smaller. Due to the irregular shape of the cracks, the detailed width values of the cracks were not accurately measured during the test. Through the authors' analysis, it may be related to the production process of the FRP tube, the fiber winding angle, and length–diameter ratio. A weak surface would be formed at the cracking position. The aforementioned phenomena have a certain relationship with the eccentricity of the specimen failure caused by the continuous increase in the core concrete strength.

3.3.2 Load–Displacement Behaviors of the Three Types of Specimens

Figure 5 shows the load–displacement behaviors of the three types of specimens. It can be seen that the core concrete under FRP tube confinement showed an approximately linear load–displacement relationship from the beginning of the test to the turning load and became nonlinear after the turning load, especially for N-CFFT and UES–CFFT (**Figures 5B,C**). It should be noted that with the increase in the early strength of core concrete, the damage of the FRP tube gradually became less, and the concrete cracking gradually became uniform. Combined with **Figure 4**, it can be obtained that the change in the horizontal confinement level had a significant indigenous effect on the damage extent of the FRP rupture area of the specimens and the crack morphology and damage height in the concrete. The change in failure modes showed that the damage of FRP tubes became slight with the increase in core concrete strength, and the failure modes of concrete changed from irregular scattered failure to uniform minor failure. The synergy of the two made the load capacity of the whole column significantly improved.

The ultimate load capacities of the three types of specimens are shown in **Table 5**. The ultimate load observed in the table has been shown in the load–displacement curves (**Figure 5**), and the average value of the three test results was taken as the ultimate load of each type of specimen. Compared with the FT, the ultimate load capacities of N-CFFT and UES–CFFT were increased by approximately 9 and 16 times, respectively. Moreover, the ultimate load capacities of UES–CFFT were 73.3% higher than those of N-CFFT. The low value of coefficient of variation (CV) shows that the variability between the test results is quite low. The maximum (CV) value of the test results listed in **Table 5** does not exceed 3%, which indicates the results can be accepted with considerable accuracy. The comparison of the ultimate loads of the three types of specimens is shown in **Figure 6**. The average change of the ultimate loads of each type of specimens directly and vividly shows the aforementioned obvious improvement effect.

3.3.3 Stress–Strain Behaviors of the Three Types of Specimens

In addition to the load–displacement relationship, experimental data between the stress and axial as well as lateral strains were also obtained. **Figure 7** shows the stress–strain behaviors of the three types of specimens. As all three specimens of each type had the

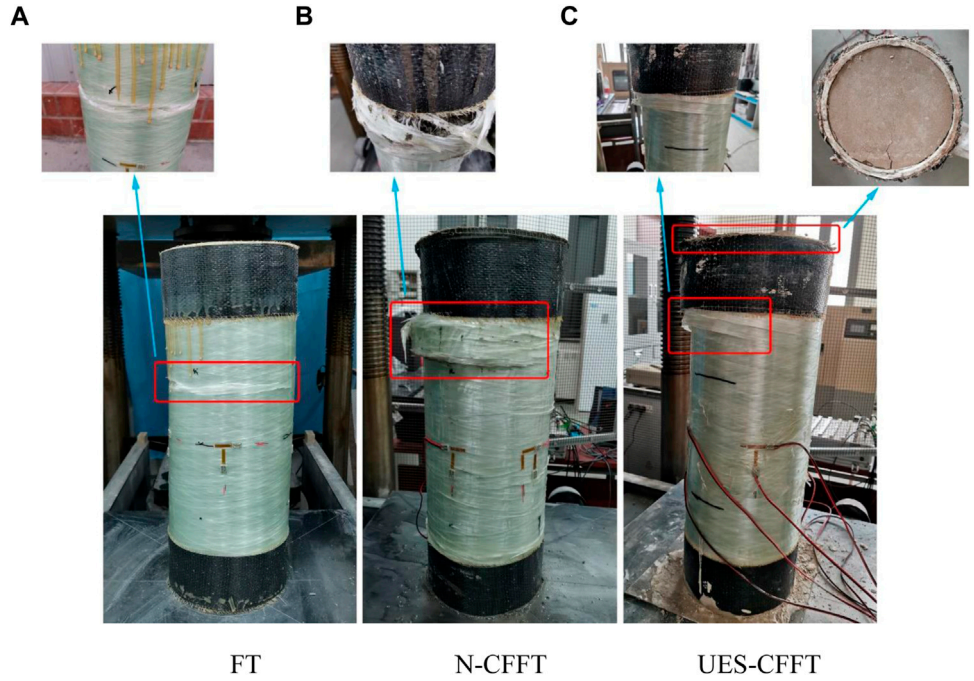

FIGURE 4 | Failure models of the three types of specimens, **(A)** FT, **(B)** N-CFFT, and **(C)** UES–CFFT.

same stress–strain trend, the most representative of these results had been selected for the convenience of the curves presentation. According to the existing research, the complete axial compression process of the CFFT can be roughly divided into three stages (Wu D. et al., 2006): the initial linear elastic stage, the middle elastic–plastic stage, and the late strengthening stage. In the present study, the failure of FT and UES–CFFT specimens occurred in the first stage, while the failure of N-CFFT specimens occurred in the second stage. Through analysis, it is possible that the confinement effect provided by the FRP tube was not sufficient compared with that of ultra-early strength concrete, leading to the early failure of UES–CFFT. Furthermore, comparing **Figures 7A2, B2, C2**, taking the lateral-to-axial strain curves of the most representative measuring point 3 in each figure as an example, it can be seen that when the lateral strain reaches its limit value, the axial strain of UES–CFFT is greatly increased compared to that of FT and N-CFFT, thus validating the above statements.

3.3.4 Compressive Strength Behaviors of the Three Types of Specimens

The compressive strengths of the three types of specimens are given in **Table 6**. The compressive strength was obtained by dividing the compressive load (*Pu*) and the cross-sectional area (*A*) of the specimens according to the recommended standard of GB/T 1448—"Fibre-reinforced plastics composites—Determination of compressive properties." The cross-sectional area (*A*) was the actual cross-sectional area. The outer diameter of all specimens was 200 mm, and the actual cross-sectional area was 31,416 mm^2 for both N-CFFT and UES–CFFT. However, the effective contact area of FT was only within the range of 6 mm thickness, and its actual cross-sectional area was 3,647 mm^2. Similarly, the average value of the three test results was taken as the compressive strength of each type of specimens. The low value of coefficient of variation (CV) indicates that the variability between test results is quite low. The maximum (CV) value of the test results listed in **Table 4** does not exceed 3%, which indicates the results can be accepted with considerable accuracy. Compared with the FT specimens, the compressive strengths of N-CFFT and UES–CFFT specimens were increased by 18.6 and 97.2%, respectively. The comparison of compressive strength of the three types of specimens is shown in **Figure 8**. It is obvious that the compressive strength increases with the increase in the early strength of the core concrete, and the compressive strength of UES–CFFT specimens is the largest.

4 THEORETICAL PREDICTION MODEL FOR THE COMPRESSIVE STRENGTH OF THE UES-CFFT

4.1 Comparison of Test Results With Predictions of Existing Models

Most of the existing CFFT models are based on a recognized characteristic that the lateral confinement of the FRP tube is capable to greatly improve the integral axial compressive strength (karbhari and Gao, 1997). The failure of CFFT composites is marked by the tensile failure of FRP in the hoop direction. The compressive strength is the basic material

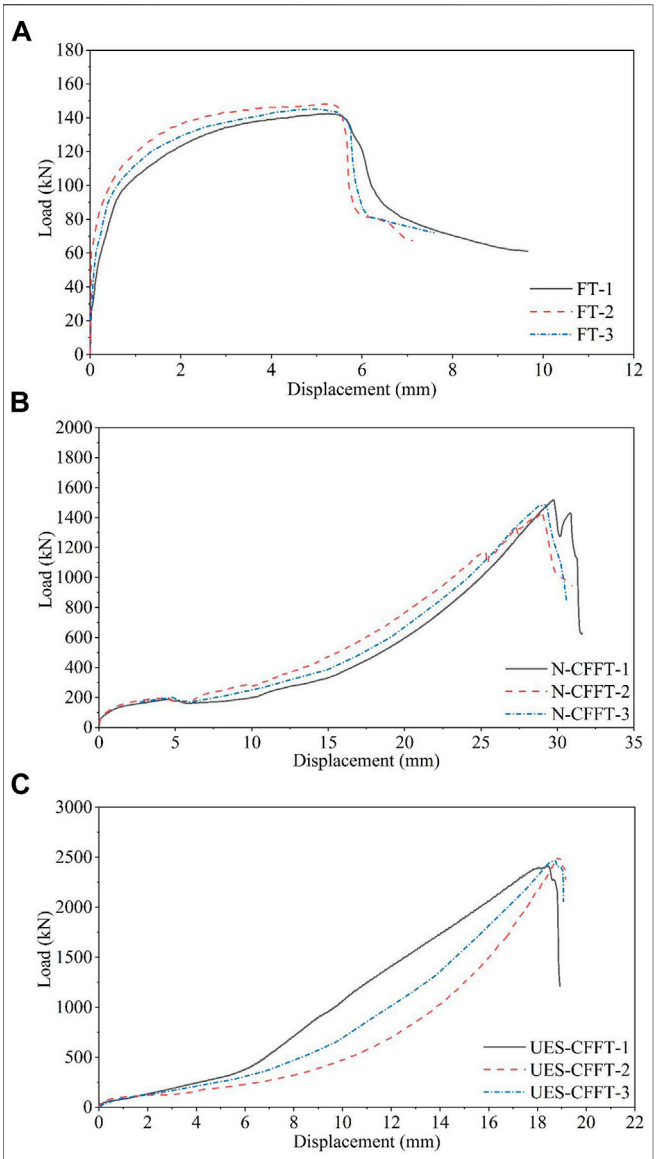

FIGURE 5 | Load–displacement variation curves of the three types of specimens, **(A)** FT, **(B)** CFFT, and **(C)** UES–CFFT.

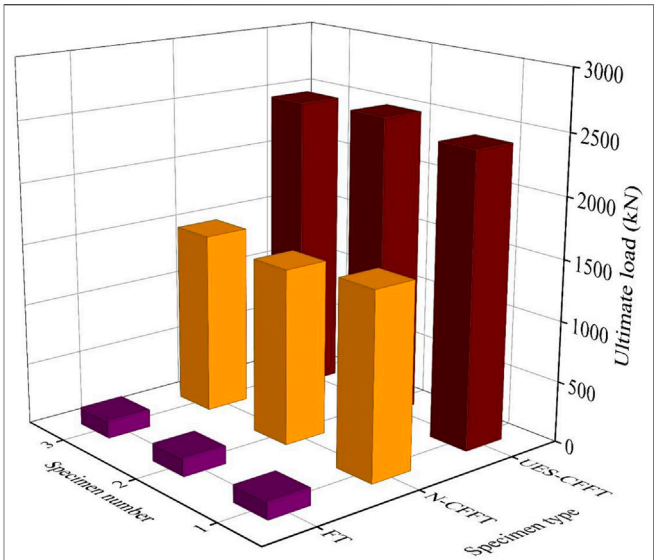

FIGURE 6 | Ultimate load comparison of the three types of specimens.

TABLE 5 | Load capacities of the three types of specimens under compression.

Specimen ID	Ultimate load (kN)	Average (kN)	Improvement (%)	CV (%)
FT-1	142			
FT-2	148	145		2.1
FT-3	145			
N-CFFT-1	1,518			
N-CFFT-2	1,437	1,481	921	2.8
N-CFFT-3	1,488			
UES-CFFT-1	2,411			
UES-CFFT-2	2,500	2,459	1,596	1.8
UES-CFFT-3	2,465			

TABLE 6 | Compressive strength results of the three types of specimens under compression.

Specimen ID	Compressive strength (MPa)	Average (MPa)	Improvement (%)	CV (%)
FT-1	38.8			
FT-2	40.5	39.7		2.1
FT-3	39.7			
N-CFFT-1	48.3			
N-CFFT-2	45.7	47.1	18.6	2.8
N-CFFT-3	47.4			
UES-CFFT-1	76.7			
UES-CFFT-2	79.6	78.3	97.2	1.8
UES-CFFT-3	78.5			

characteristic to evaluate the applicability of CFFT composites as concrete compression members. In recent years, researchers have put forward many models and analysis methods through a large number of experiments on the axial compression performance of CFFT specimens, several of which take the following form:.

$$\frac{f'_{cc}}{f'_{co}} = 1 + k_1 \frac{f_l}{f'_{co}}, \tag{1}$$

where f'_{cc} and f'_{co} are the compressive strengths of the confined and the unconfined concrete, respectively; f_l is the lateral confining pressure; and k_1 is the confinement effectiveness coefficient. This form was first proposed by Richart et al. (Richart, 1928) and suggested by Fardis and Khalili (1982) (Fardis and Khalili, 1982) that it could be directly used for the CFFT. For the application to the

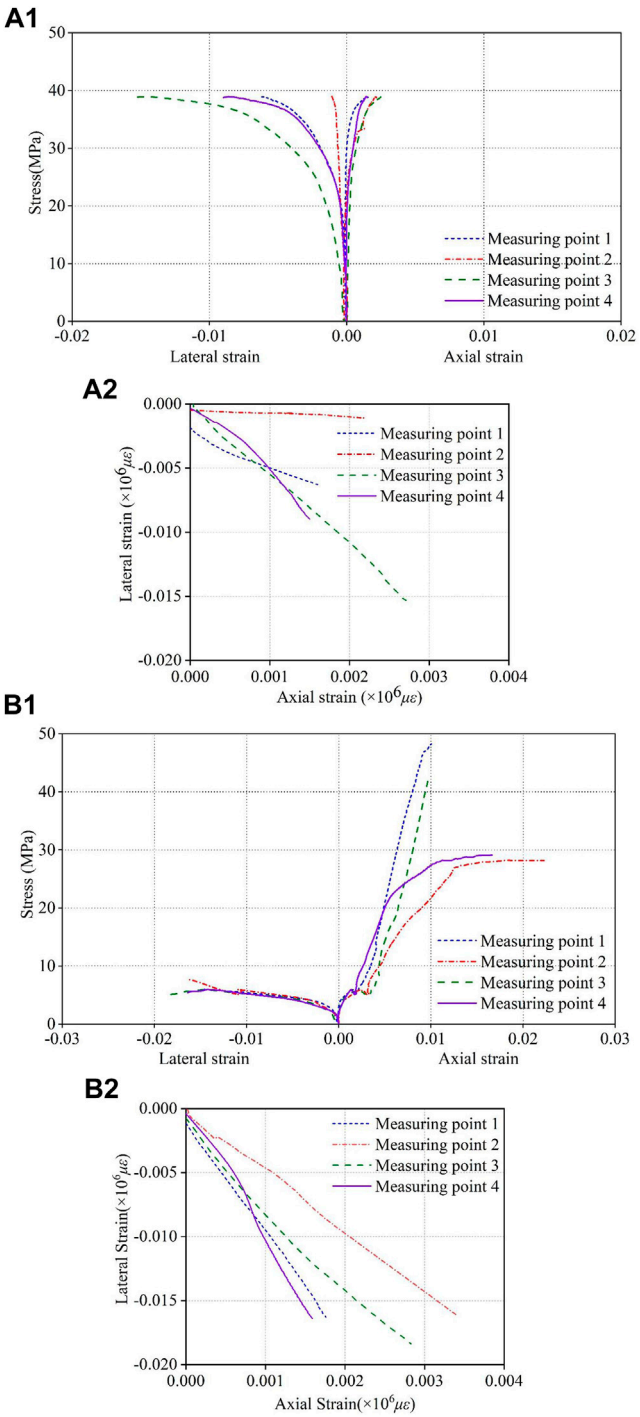

FIGURE 7 | Stress–strain curves of the three types of specimens **(A1, B1,** and **C1)**, Lateral-to-axial strain curves of the three types of specimens **(A2, B2, C2)**.

CFFT, f_l can be related to the amount and strength of the FRP as follows:

$$f_l = \frac{2E_{frp}t\varepsilon_{h,rup}}{d}, \tag{2}$$

where f_l is the local value of the lateral confining pressure, E_{frp} is the elastic modulus of the FRP in the hoop direction, t is the local nominal thickness of the FRP, $\varepsilon_{h,rup}$ is the local hoop strain from the strain gauge, and d is the diameter of the whole cylinder specimens (Lam and Teng, 2002; Lam and Teng, 2004).

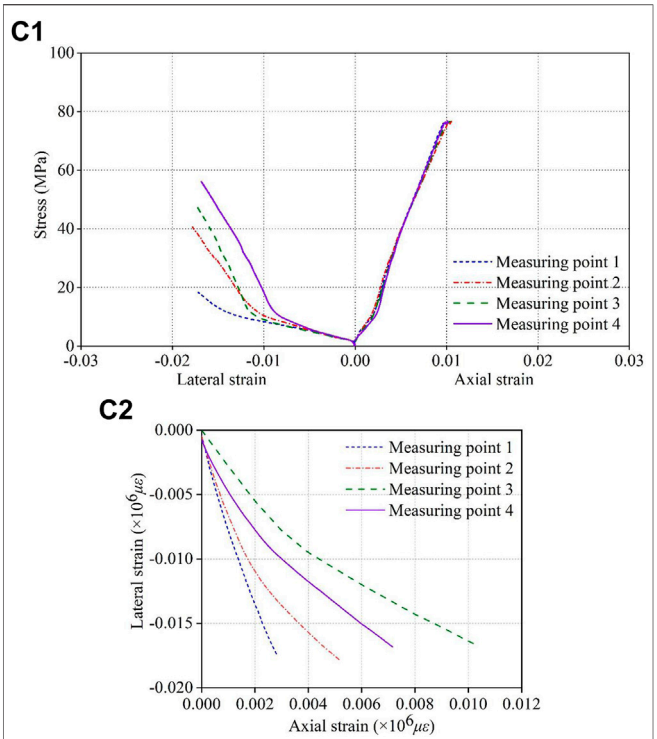

FIGURE 7 | (Continued).

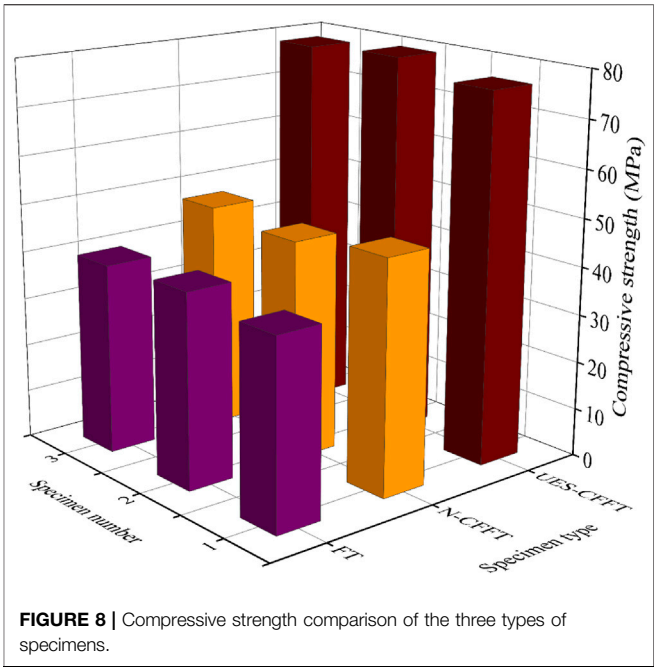

FIGURE 8 | Compressive strength comparison of the three types of specimens.

In these models proposed by Saaman et al. (Samaan et al., 1998) and Saafi et al. (1999) (Saafi et al., 1999), k_1 was not a constant but instead was dependent on either f_l/f'_{co} or f_l. The compressive performance of the CFFT model exhibits typical bilinear response (Karbhari and Gao, 1997; Mirmiran and Shahawy, 1998; Samaan et al., 1998; Saafi et al., 1999). Saaman et al. (Samaan et al., 1998) used and calibrated the four-parameter stress–strain relationship proposed by Richard and Abbott (Richard and Abbott, 1975) to represent this response. Test results indicated a bilinear response in which an initial softening or yielding occurred at the level of the unconfined strength of concrete, and the secondary slope was then proportional to the stiffness of the confining jacket. Considering the stiffness of the confining mechanism, a simple confinement model was proposed to predict the response of the CFFT in both the axial and lateral directions. Saafi et al. (Saafi et al., 1999) tested 30 concrete cylinders (18 CFFT and 12 plain concrete) and analyzed the experimental results. Equations to predict the compressive strength and failure, and the entire stress–strain curve of the CFFT were developed. The lateral strain was considered in the proposed equations. By extrapolating the ultimate conditions (i.e., $\varepsilon_l = \varepsilon_{fu}$), the equations using the current axial stress and strain as the current lateral strain functions were obtained. These equations were obtained by the best fit of the experimental results, which can be used to explain the ever-increasing confinement pressure imposed by FRP.

In 2002, Lam and Teng (Lam and Teng, 2002) had reviewed existing strength models for the CFFT and compared with available experimental data collected from an extensive literature survey. They proposed a new simple model for the prediction of the strength of CFFT based on the analysis of existing test results in the end.

Five models were proposed to predict the axial strength enhancement rate of the CFFT (f'_{cc}/f'_{co}) by comparing the

TABLE 7 | Summary of the models used to predict peak axial strength of test specimens.

Model	Peak strength equation
Samaan et al. (Samaan et al., 1998)	$\frac{f'_{cc}}{f'_{co}} = 1 + k_1\frac{f_l}{f'_{co}}, k_1 = 6.0f_l^{-0.3}$
Saafi et al. (Saafi et al., 1999)	$\frac{f'_{cc}}{f'_{co}} = 1 + k_1\frac{f_l}{f'_{co}}, k_1 = 2.2(\frac{f_l}{f'_{co}})^{-0.16}$
Lam and Teng (Lam and Teng, 2003)	$\frac{f'_{cc}}{f'_{co}} = 1 + k_1\frac{f_l}{f'_{co}}, k_1 = 3.5$
Jiang and Teng (Jiang and Teng, 2006)	$\frac{f'_{cc}}{f'_{co}} = 1 + 3.5(\frac{E_l}{(f'_{co}/\varepsilon_{co})} - 0.01)(\frac{\varepsilon_{h,rup}}{\varepsilon_{co}})$
Tamuzs et al. (Tamuzs et al., 2006a; Tamuzs et al., 2006b)	$\frac{f'_{cc}}{f'_{co}} = 1 + k_1\frac{f_l}{f'_{co}}, k_1 = 4.2$

TABLE 8 | Test results.

Specimen	f_{co} (MPa)	ε_{co}	f_{cc} (MPa)	$\varepsilon_{h,rup\ avg}$
N-CFFT-1	1.8	0.10	48.3	0.017
N-CFFT-2	1.9	0.09	45.7	0.015
N-CFFT-3	1.8	0.11	47.4	0.016
UES–CFFT-1	8.1	0.11	76.7	0.015
UES–CFFT-2	7.8	0.10	75.9	0.014
UES–CFFT-3	8.3	0.12	76.3	0.017

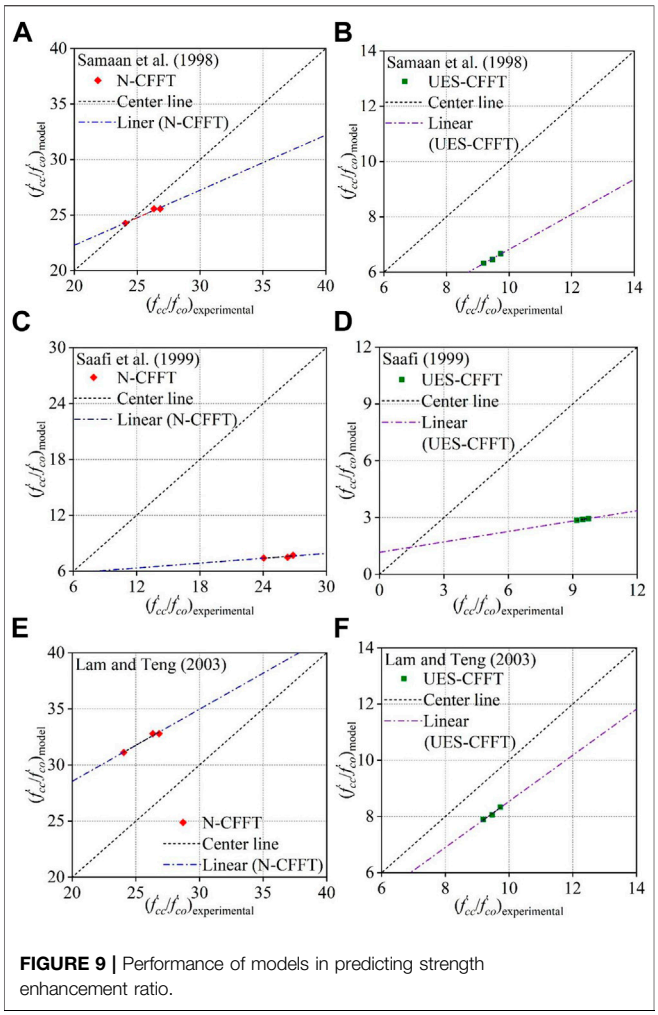

FIGURE 9 | Performance of models in predicting strength enhancement ratio.

experimental results of the present study. The five models shown in **Table 6** were selected from the comprehensive model review studies reported in Ozbakkaloglu et al. (Ozbakkaloglu et al., 2013). The models used in this article were based on three main factors. First, the models were selected for their ability to predict the ultimate strength. The second criterion was the model format, which was presented in a simple closed-form equation format only when the model was initially considered. Finally, the models were selected with proven good performance for the CFFT assessed in Ozbakkaloglu et al. (Ozbakkaloglu et al., 2013; Vincent and Ozbakkaloglu, 2013).

To effectively evaluate the performance of these models, three statistical indicators were cited in this article: the mean square error (MSE), the average absolute error (AAE), and the linear trend slope (LTS). The first two, as the statistical indicators of modeling accuracy, the lower the value, the better is the performance of the model. They were defined by **Eq. 3** and **Eq. 4**, respectively. The third one, determined by a regression analysis, was used to describe the associated average overestimation or underestimation of the model, where an overestimation was represented by a linear trend slope greater than 1 (Vincent and Ozbakkaloglu, 2013). **Table 7** presents the summary of the model assessment.

$$MSE = \sum_{i=1} n \frac{(\mathrm{mod}_i - \exp_i)^2}{N} \text{ and} \tag{3}$$

$$AAE = \frac{\sum_{i=1}^{n} \left| \frac{\mathrm{mod}_i - \exp_i}{\exp_i} \right|}{N}. \tag{4}$$

Table 8 summarizes the test results of the N-CFFT and UES–CFFT specimens, of which (f'_{co}) and (ε_{co}) have been mentioned in **Table 2**. Besides, the ultimate strength of confined concrete ($f_{,cc}$) and the FRP hoop rupture strain ($\varepsilon_{h,rup\ \ avg}$) were also reported. **Figure 9** shows the comparisons between the experimental results of ultimate strength and the existing model predictions. It can be seen from the model comparisons that most models have certain scatter in predicting the ultimate strength. Among them, when the models were applied to the N-CFFT specimens, the prediction performance of the model proposed by Samaan et al. (Samaan et al., 1998) was better. When the models were applied to the UES–CFFT specimens, the prediction performance of the model proposed by Tamuzs et al. (Tamuzs et al., 2006a; Tamuzs et al., 2006b) was better. As can be seen from **Table 9**, in the prediction models applied to the N-CFFT specimens, the error statistical indicators MSE and AAE of the model proposed by Samaan et al. (Samaan et al., 1998) are the lowest. In the prediction models applied to the UES–CFFT specimens, the error statistical indicators MSE and AAE of the model proposed by Tamuzs are the lowest. Besides, the recorded value of LTS is 1.06, which is the closest to 1 among the five models.

4.2 Proposed New Model

It can be seen that most models had high error levels when they were applied to both CFFT and UES–CFFT specimens. On the one hand, the current models could not provide sufficient accuracy in predicting the ultimate strength conditions of N-CFFT and UES–CFFT specimens. On the other hand, the N-CFFT and UES–CFFT specimens in the present study were tested after the core concrete was cured for 5 hours and zero, respectively. The difference of the core concrete strength was relatively large, resulting in a large error in the prediction model to predict the two types of specimens at the same time. At present, there have been a large number of strength prediction models for the N-CFFT. Based on the aforementioned observations, a compression strength prediction model for the UES–CFFT was proposed in this article. Using a regression analysis of the experimental data, an equation for k_1 can be calculated as follows:

$$k_1 = 3.94. \tag{5}$$

By substituting **Eq. 5** into **Eq. 1**, the compressive strength at every point of the second zone is given by the following equation:

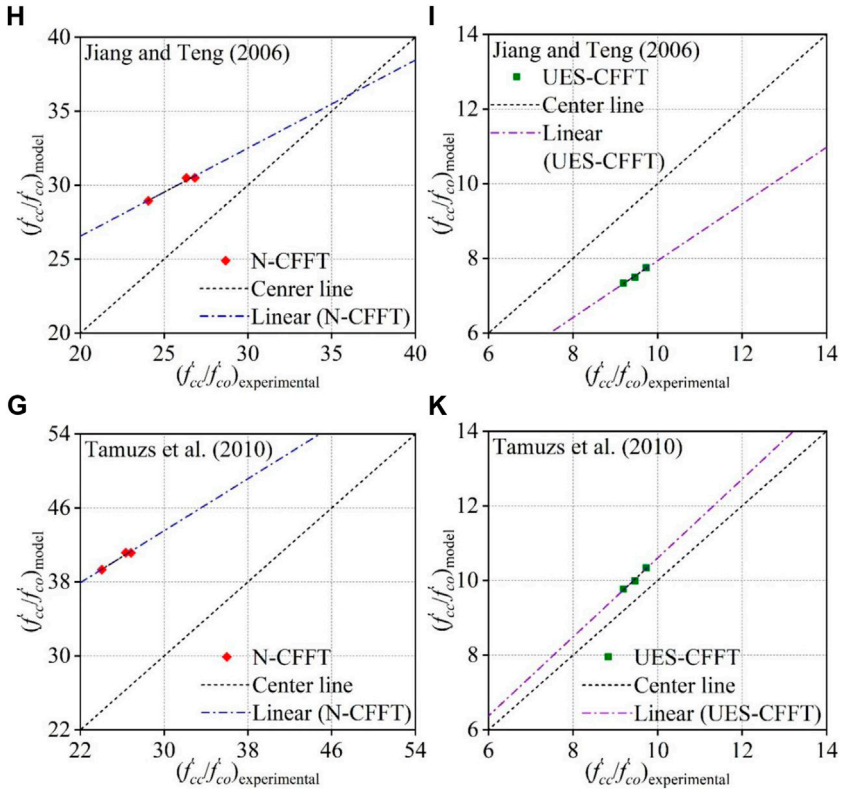

FIGURE 9 | (Continued).

TABLE 9 | Statistics on models of strength enhancement ratios of test specimens.

Model	Concrete type	Prediction of f′ cc/f′ co		
		MSE	AAE	LTS
Samaan et al. (Samaan et al., 1998)	N-CFFT	0.76	0.03	0.50
	UES–CFFT	8.89	0.31	0.63
Saafi et al. (Saafi et al., 1999)	N-CFFT	330.01	0.70	0.09
	UES–CFFT	43.08	0.69	0.18
Lam and Teng (Lam and Teng, 2003)	N-CFFT	42.36	0.25	0.64
	UES–CFFT	1.87	0.14	0.82
Jiang and Teng (Jiang and Teng, 2006)	N-CFFT	18.20	0.17	0.60
	UES–CFFT	3.74	0.20	0.76
Tamuzs et al. (Tamuzs et al., 2006a; Tamuzs et al., 2006b)	N-CFFT	225.39	0.58	0.7
	UES–CFFT	0.33	0.06	1.06

$$\frac{f'_{cc}}{f'_{co}} = 1 + 3.94\frac{f_l}{f'_{co}}. \quad (6)$$

The comparison between the experimental results of ultimate strength and the proposed new model predictions is presented graphically in **Figure 10**. As can be seen, **Figure 10** shows a good agreement between the experimental results with the predicted compressive strength results of the tested specimens. Besides, the error statistical indicators MSE and AAE of the proposed new model are both close to 0 by calculation, indicating the validity and accuracy of the results.

5 CONCLUSION

The compressive performance of N-CFFT with 5-hour curing time and UES–CFFT with zero curing time was experimentally

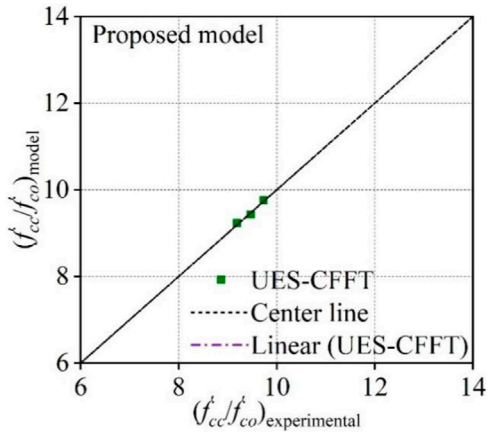

FIGURE 10 | Performance of the proposed new model in predicting strength enhancement ratio.

studied. Based on the results and discussion in this article, the following conclusions can be drawn as follows:

(1) The FRP tube is an effective confinement manner, which can greatly improve the ultimate compressive strength and ductility of core concrete.
(2) The combination of rapid early strength improvement of UESC and the confinement effect of the FRP tube was testified to be effective. The ultimate compressive strength of UES–CFFT with zero curing time reached 78.3 MPa, which was 66.2 and 97.2% higher than that of FT and N-CFFT with 5-hour curing time. This can be conducive to rapid construction operations in road engineering, avoiding problems such as traffic inconvenience.
(3) Few of the existing analysis models involved the prediction of the ultimate strength of UES–CFFT with zero curing time, and there would be some errors in the test results used to predict in this article. Therefore, based on the analysis of the existing test results, a modified simple model for predicting the ultimate strength of UES–CFFT with zero curing time was proposed, and its accuracy was proved to be high (Standardization Administration of the People's Republic of China, 2005).

DATA AVAILABILITY STATEMENT

The original contributions presented in the study are included in the article/Supplementary Material; further inquiries can be directed to the corresponding author.

AUTHOR CONTRIBUTIONS

YL involved in supervision, conception, experimental work, data analysis, and writing draft, review, and editing; J-ZX helped with validation, data analysis, and writing draft, review, and editing; and J-LY assisted with experimental work, data analysis.

ACKNOWLEDGMENTS

The authors are grateful to the financial support from the National Natural Science Foundation of China (NSFC 51908012) and the Postdoctoral Research Foundation of China (2019M660962).

REFERENCES

Astm, D. (2015). *Standard Test Methods for Constituent Content of Composite Materials*. Conshohocken, PA): ASTM West.

Fam, A., Flisak, B., and Rizkalla, S. (2001). "FRP Tubes Filled with concrete and Subjected to Axial Loads, Bending and Combined Loads," in *FRP Composites in Civil EngineeringProceedings of the International Conference on FRP Composites in Civil Engineering* (Hong Kong: Hong Kong Institution of Engineers, Hong Kong Institution of Steel Construction).

Fardis, M. N., and Khalili, H. H. (1982). FRP-encased concrete as a Structural Material. *Mag. Concrete Res.* 34 (121), 191–202. doi:10.1680/macr.1982.34.121.191

Jiang, T., and Teng, J. (2006). *Strengthening of Short Circular RC Columns with FRP Jackets: A Design Proposal*. Miami, FL, USA: Semantic Scholar.

Karbhari, V. M., and Gao, Y. (1997). Composite Jacketed Concrete under Uniaxial Compression-Verification of Simple Design Equations. *J. Mater. civil Eng.* 9 (4), 185–193. doi:10.1061/(asce)0899-1561(1997)9:4(185)

Lam, L., and Teng, J. G. (2003). Design-oriented Stress–Strain Model for FRP-Confined concrete. *Construction building Mater.* 17 (6-7), 471–489. doi:10.1016/s0950-0618(03)00045-x

Lam, L., and Teng, J. G. (2002). Strength Models for Fiber-Reinforced Plastic-Confined Concrete. *J. Struct. Eng.* 128 (5), 612–623. doi:10.1061/(asce)0733-9445(2002)128:5(612)

Lam, L., and Teng, J. G. (2004). Ultimate Condition of Fiber Reinforced Polymer-Confined Concrete. *J. Compos. Constr.* 8 (6), 539–548. doi:10.1061/(asce)1090-0268(2004)8:6(539)

Li, J., and Xue, Y. (2004). Experimental Study on Concrere-Filled FRP Tube Composite Structure. *Fiber Reinforced Plastics/Composites* 30 (6), 7–9. doi:10.3969/j.issn.1003-0999.2004.06.002

Mirmiran, A., and Shahawy, M. (1995). "A Novel FRP-concrete Composite Construction for the Infrastructure," in *Restructuring: America and beyond:* (Boston, MA, United States: ASCE), 1663–1666.

Mirmiran, A., and Shahawy, M. (1997). Behavior of concrete Columns Confined by Fiber Composites. *J. Struct. Eng.* 123 (5), 583–590. doi:10.1061/(asce)0733-9445(1997)123:5(583)

Mirmiran, A., Shahawy, M., and Beitleman, T. (2001). Slenderness Limit for Hybrid FRP-concrete Columns. *J. Compos. Constr.* 5 (1), 26–34. doi:10.1061/(asce)1090-0268(2001)5:1(26)

Ozbakkaloglu, T., Lim, J. C., and Vincent, T. (2013). FRP-confined concrete in Circular Sections: Review and Assessment of Stress-Strain Models. *Eng. Structures* 49, 1068–1088. doi:10.1016/j.engstruct.2012.06.010

Richard, R. M., and Abbott, B. J. (1975). Versatile Elastic-Plastic Stress-Strain Formula. *J. Engrg. Mech. Div.* 101 (4), 511–515. doi:10.1061/jmcea3.0002047

Richart, F. E. (1928). *A Study of the Failure of Concrete under Combined Compressive Stresses*. Bulletin: University of Illinois, Engineering Experimental Station.

Saafi, M., Toutanji, H. A., and Li, Z. (1999). Behavior of Concrete Columns Confined with Fiber Reinforced Polymer Tubes. *ACI Struct. J.* 96 (4), 500–509. doi:10.14359/652

Samaan, M., Mirmiran, A., and Shahawy, M. (1998). Model of Concrete Confined by Fiber Composites. *J. Struct. Eng.* 124 (9), 1025–1031. doi:10.1061/(asce)0733-9445(1998)124:9(1025)

Standardization Administration of the People's Republic of China (2005). *Fiber-reinforced Plastics Composites-Determination of Compressive Properties*. GB/T1448-2005. Beijing, China.

Tamuzs, V., Tepfers, R., and Sparnins, E. (2006a). Behavior of concrete Cylinders Confined by Carbon Composite 2. Prediction of Strength. *Mech. Compos. Mater.* 42 (2), 109–118. doi:10.1007/s11029-006-0022-7

Tamuzs, V., Tepfers, R., Zile, E., and Ladnova, O. (2006b). Behavior of concrete Cylinders Confined by a Carbon Composite 3. Deformability and the Ultimate Axial Strain. *Mech. Compos. Mater.* 42 (4), 303–314. doi:10.1007/s11029-006-0040-5

Tasdemir, M. A., Tasdemir, C., Akyüz, S., Jefferson, A. D., Lydon, F. D., and Barr, B. I. G. (1998). Evaluation of Strains at Peak Stresses in concrete: a Three-phase Composite Model Approach. *Cement and Concrete Composites* 20 (4), 301–318. doi:10.1016/s0958-9465(98)00012-2

Teng, J., Yu, T., Wong, Y., Dong, S., and Yang, Y. (2006). Behavior of Hybrid FRP-Concrete-Steel Tubular Columns:Experimental and Theoretical Studies. *Progress Steel Building Structures* 8 (5), 1–7. doi:10.3969/j.issn.1671-9379.2006.05.001

Vincent, T., and Ozbakkaloglu, T. (2013). Influence of concrete Strength and Confinement Method on Axial Compressive Behavior of FRP Confined High- and Ultra High-Strength concrete. *Composites B: Eng.* 50, 413–428. doi:10.1016/j.compositesb.2013.02.017

Wu, Z. (2007). "Some Key Issues and Techniques in Strengthening Structures with Bonded FRP Composites," in *Articles of the First National Symposium on Design and Construction Technology of Existing Structure Reinforcement and Reconstruction* (Beijing).

Wu, G., and Lv, Z. (2003). Study on the Stress-Strain Relationship of FRP-Confined concrete Circular Column without a Strain-Softening Response. *J. Building Structures* 24 (5), 1–9. doi:10.3321/j.issn:1000-6869.2003.05.001

Wu, D., Yang, S., Tang, G., and Zhou, T. (2006). Axial Compression Ultimate Strength of FRP Tube Reinforced concrete Structure. *Fiber Composites* 23 (1), 15–17. doi:10.3969/j.issn.1003-6423.2006.01.005

Wu, G., Wu, Z., and Lv, Z. (2006). Study of the Stress-Strain Relationship of FRP—Confined Circular concrete Column with a Strain-Softening Response. *China Civil Eng. J* 39 (11), 7–14. 76. doi:10.3321/j.issn:1000-131X.2006.11.002

Xie, Q., Zheng, P., Xue, J., and Yang, Y. (2012). *Research Status and Prospects on FRP—concrete Tubular Columns*. Chengdu, China: Sichuan Building Science.

Zhuo, W., and Fan, L. (2005). The Concept and Seismic Performance of GFRP Tube - concrete Composite Piers. *J. Fuzhou University(Natural Sci. Edition)* 33 (1), 73–79. doi:10.3969/j.issn.1000-2243.2005.01.018

Conflict of Interest: The authors declare that the research was conducted in the absence of any commercial or financial relationships that could be construed as a potential conflict of interest.

Publisher's Note: All claims expressed in this article are solely those of the authors and do not necessarily represent those of their affiliated organizations, or those of the publisher, the editors, and the reviewers. Any product that may be evaluated in this article, or claim that may be made by its manufacturer, is not guaranteed or endorsed by the publisher.

Copyright © 2022 Liu, Xie and Yan. This is an open-access article distributed under the terms of the Creative Commons Attribution License (CC BY). The use, distribution or reproduction in other forums is permitted, provided the original author(s) and the copyright owner(s) are credited and that the original publication in this journal is cited, in accordance with accepted academic practice. No use, distribution or reproduction is permitted which does not comply with these terms.